Generalization of the singum model for the elasticity prediction of lattice metamaterials and composites

Huiming Yin[1]

[1]Department of Civil Engineering and Engineering Mechanics, Columbia University, 610 Seeley W. Mudd 500 West 120th Street, New York, 10027. Email: yin@civil.columbia.edu

ABSTRACT

The recently developed singum model is extended to lattice metamaterials and composites for prediction of the effective elasticity based on the stiffness of the lattice components and the structure of the lattice, in which the load is transferred through the lattice network represented by unit cells that can contain one or more singums. The equilibrium of the singums is considered under a displacement variation, and the relation between the variations of averaged stress and strain can be evaluated to predict the elasticity. It is proved that the stiffness of any unit cells is the same as the primitive cell. A generalized formulation is developed to calculate the effective elasticity of lattice metamaterials and composites, which reflects the symmetry and anisotropic feature of the lattice more accurately. A hydrostatic load does not change the shape of the singum but changes its elasticity, although the bonds are linear elastic. The formulation discloses the prestress-dependent elasticity for lattice metamaterials. When a large uniform biaxial tension is applied, a honeycomb lattice can exhibit a negative Poisson's ratio under a pre-tension. The case studies of auxetic and body-centered cubic lattices are conducted to demonstrate the negative Poisson's ratio and anisotropic elasticity, respectively.

INTRODUCTION

The recently developed singum model (Yin 2022) uses the Wigner-Seitz (WS) cells of a crystal lattice to represent a continuum solid, so that the singular point forces between atoms can be transformed into the contacting stress between the continuum particle. By applying a displacement variation, from the relationship between the virtual stress and strain, we obtain the elastic constants. This procedure can be applied to general lattice networks, which exist in nature or metamaterials or composites. For example, polymer macromolecules form the solid in a certain lattice pattern in the three-dimensional (3D) space (Boyce and Arruda 2000). Auxetic metamaterials can be fabricated with a two-dimensional (2D) or 3D lattices showing negative Poisson's ratio for the overall materials (Lakes 1987; Saxena et al. 2016). Textile or lattice based composites can be lightweight and strong for multifunctional material applications (Mouritz et al. 1999; Gregg et al. 2018). Particularly, the additive manufacturing has made it possible to fabricate lattice materials straightforwardly.

When the one dimensional (1D) bonds connect with each other into a lattice, which forms a 2D or 3D solid at the macroscale, it creates new mechanics and physics of solids as the stress transfer through the lattice is different from the continuum solids (Šturcová et al. 2005). The classical micromechanical models are often based on the stress homogenization of the continuous material phases and provide elasticity prediction based on the volume fraction and mechanical properties of each material phase (Mura 1987; Yin and Zhao 2016). Particularly, when micromechanics-based models (Ju and Chen 1994; Tucker III and Liang 1999) treated the 1D components such as fibers as dispersed reinforcements, the reinforcement nature of the force transfer through the network cannot be captured. Although many papers in the literature addressed specific lattices with numerical simulations (Li et al. 2003; Chen et al. 2013; Gao et al. 2021), the models highly depended on the material design and computational resources. However, an analytical formulation between the microstructure of lattices and their effective elasticity has not been developed yet.

This paper generalizes the singum model (Yin 2022) to lattice metamaterials and composites, which are formed with a network of nodes linked by elastic bars. It provides a general modeling framework for the prediction of the effective elasticity of a material exhibiting lattice structures. The model can also be extended to fiber-reinforced composites with such a lattice network embedded in a soft or elastic matrix. The modeling framework can be implemented straightforwardly with the primitive cell of complex lattices, and thus transform a network system into a continuum body with effective elasticity.

This paper first reviews the singum construction for a honeycomb lattice containing elastic bond members (Yin 2022) and discuss the equilibrium of singums under a variation of displacement field corresponding to a uniform strain of the lattice. Although the simplified singum model (Yin 2022) was developed for a primitive cell containing a single node, when a primitive cell contains two singums, a single singum may not maintain equilibrium. This paper adopts the variational method, in which the equilibrium and volume change of the singums with the strain variation are taken into account and a new stiffness of the regular honeycomb lattice is derived. The singum model is generalized to more complex lattices after some theoretical preparation with five lemmas and one

theorem. The generalized singum model is used to investigate the regular honeycomb lattice under a 2D hydrostatic load. The stability and prestress-dependent elasticity of the lattice is discussed. Two case studies are conducted to demonstrate the model applications to lattice metamaterials and composites.

FORMULATION

The singum modeling framework for honeycomb lattices

In the previous paper (Yin 2022), we used a regular honeycomb lattice in a two-dimensional (2D) space to demonstrate the singum construction. In Fig. 1(a), the lattice consists of atoms and bonds, which was replaced by triangular singums to fill the space. We constructed the singum by the Voronoi decomposition of the lattice. Actually, the combination of two singums A and B with a mirror symmetry can represent the lattice and serve as the primitive cell. The simplified singum model used one atom to represent the whole honeycomb lattice, which shows an isotropic stiffness tensor in the 2D plane with the magnitude depending on the potential function $V(r)$ with r being the bond length. However, a face center cubic (FCC) lattice exhibits a cubic symmetry of the stiffness tensor.

This paper will generalize the singum model to elastic lattices made of elastic bars linked by nodes with the same geometric features and revisit the appropriateness of using a single singum to represent the whole lattice, which shows a correction for higher accuracy. Here we use the same language to call a bar linking two closest nodes as a bond, which can be defined as a vector $\mathbf{r} = \mathbf{x}^1 - \mathbf{x}^0$ with the length $r = |\mathbf{x}^1 - \mathbf{x}^0|$. Here $\mathbf{x}^0$ represents the singum node and $\mathbf{x}^1$ represents another node bonded to the singum. Similarly, we can build up the singum model with the following assumptions:

1. The interaction between nodes is governed by the bond's potential function $V(r)$.
2. The interaction between two neighboring singums is through the surface stress vector along their interface edge, and is equivalent to the bond force between the two nodes.
3. All forces on the boundary or the center of WS cell of the lattice, which are seen on the nodes and bond cutting points, will be conserved on the singum with a homogeneous elasticity $\mathbf{C}$.

The force of a bond can be written as

$$F_i = \frac{dV}{d\mathbf{r}} = V_{,r} n_i \tag{1}$$

where $\mathbf{n} = \frac{\mathbf{x}^1 - \mathbf{x}^0}{|\mathbf{x}^1 - \mathbf{x}^0|}$. Here the tensile force in the bond is taken as positive along $\mathbf{n}$ to be consistent with the sign convention of stresses. For an elastic bar with a Young's modulus E, length r_0, and cross-sectional area A at the stress-free state, the potential function can be written as

$$V(r) = \frac{k}{2}(r - r_0)^2 \tag{2}$$

where

$$k = \frac{EA}{r_0} \tag{3}$$

For simplicity and clarity, this paper assumes all bars share the same E, r_0, and A, so that we can use a single potential function for all bonds, although the model can

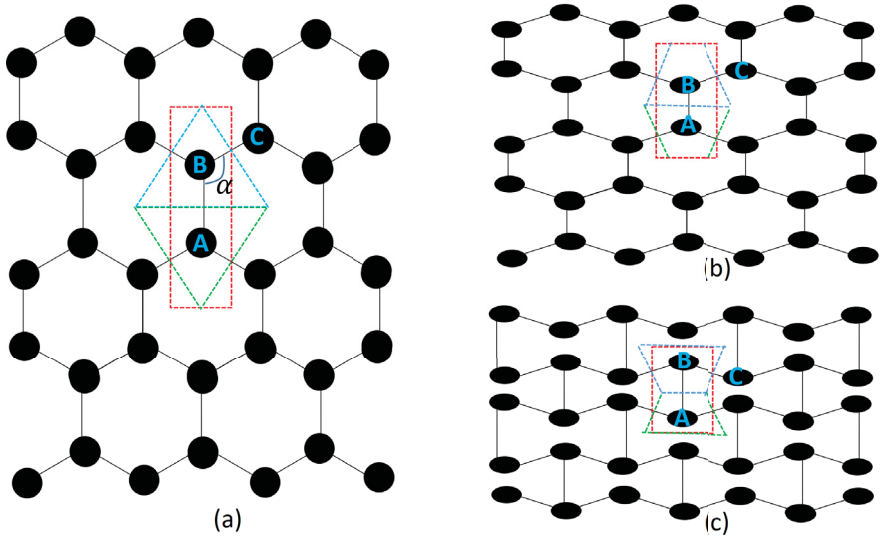

Fig. 1. The singum construction on twisted lattices with the same bond length: (a) a regular honeycomb lattice with $\alpha = \frac{2\pi}{3}$, (b) a twisted honeycomb lattice with $\frac{\pi}{2} \leq \alpha < \frac{2\pi}{3}$, and (c) a twisted honeycomb lattice with $\frac{\pi}{3} \leq \alpha < \frac{\pi}{2}$

be extended to different bars that requires the different potential functions accordingly. Moreover, we assume k will keep constant with the deformation. For example, when the bars are actually made of linear springs, the actual spring coefficient can be directly used in Eq. (2) and Eq. (3) is unnecessary.

The lattice in Fig. 1(a) can be represented by two nodes, say A and B, which form a primitive cell, i.e. the smallest unit cell. For example, the red rectangular cell can perfectly fill the space with the exact same pattern, but A and B show a mirror symmetry of the connection pattern, and a single node of them cannot represent the lattice. On the other hand, the selection of the surroundings of A and B is not unique. Following the singum construction, the Voronoi decomposition makes a blue triangle for B and a green triangle for A, which can be combined into a primitive cell to fill the space as well. However, we can see the bond cutting points are the intersection of the two unit cells. Therefore, the choice of primitive cell shape cannot change the lattice nature.

Particularly, when the lattice is compressed, the lattice shape may change into Fig. 1(b). The primitive cell can map to the deformed WS cells, which shows different shape of the singums, changing the shape from a regular triangle to an isosceles trapezoid. Moreover, we can purposely fabricate a lattice in Fig. 1(c), whose singum shape become a downward isosceles trapezoid. The lattice is an example of an auxetic lattice which exhibits a negative Poisson's ratio. From this arises a question: whether can a single singum represent the whole lattice?

To answer this question, we will first go through the case of a single singum, and then generalize the singum modeling to the primitive cell in the next subsection. By comparison of the two scenarios, we can conclude that it is necessary to consider the whole primitive cell instead of a single singum for accurate prediction.

Notice the lattice or framework in Fig. 1(a) is not statically determinate. However, if

the boundary nodes are framed or a periodic boundary condition is applied, the structure becomes stable as each internal node connects with three nodes, so that the stiffness of the lattice can be evaluated. The frame can serve as the loading plate to the lattice for elastic testing. A displacement variation corresponding to a uniform strain can be applied to the loading plate, which will generate a uniform stress on average through the solid as well. From the relationship of the stress and strain, the stiffness can be measured. Prestress can also be applied to the lattice through the frame, so that the effective stiffness changing with the bond length or prestress can also be evaluated.

Before the lattice is framed with loading plates, its pattern can be twisted by changing the angle between AB and BC, namely α without changing the bonds. When $\alpha = \frac{2\pi}{3}$, the lattice exhibits a regular honeycomb pattern and a triangular singum. When $\frac{\pi}{2} \le \alpha < \frac{2\pi}{3}$, the singum at B becomes an upward isosceles trapezoid in Fig. 1(b). When $\frac{\pi}{3} \le \alpha < \frac{\pi}{2}$, the singum at B becomes a downward isosceles trapezoid in Fig. 1(c), which is auxetic. With the decrease of α from $\frac{2\pi}{3}$ toward $\frac{\pi}{3}$, the density of the lattice increase about three times. Once the lattice pattern is fixed at a certain value of α and stretched to a bond length of $2l_p$ and framed into a 2D plate, the effective elasticity of the lattice can be evaluated.

The simplified singum model (Yin 2022) applied a virtual displacement on the lattice but ignored the effect of the virtual displacement on the equilibrium and volume change of the singum, so that the result may not capture the physics of the negative Poisson's ratio at all. In this paper, given a displacement variation in a unit cell, the singum modeling framework remains the same, including the following steps:

1. Use the Voronoi decomposition to separate the lattice into WS cells, which define the geometry of singums.
2. Given a representative singum, we can set up the local coordinate at the central node and define $\mathbf{x}^I$, $\mathbf{n}^I$, and $\mathbf{F}^I$, etc.
3. Given a displacement variation, which is corresponding to a uniform strain of the lattice, we can calculate the average stress caused by the displacement variation.
4. Using the relationship between the stress and strain variations, we can derive effective stiffness $\mathbf{C}$.

For a regular honeycomb lattice with $\alpha = \frac{2\pi}{3}$, using a virtual displacement in Step 3, the previous paper provided the elasticity of the singum (Yin 2022) as

$$C_{ijkl} = \frac{1}{4\sqrt{3}l_p t_0}\left[(2l_p V_{,rr} - V_{,r})\delta_{ij}\delta_{kl} + \left(2l_p V_{,rr} + 3V_{,r}\right)\left(\delta_{ik}\delta_{jl} + \delta_{jk}\delta_{il}\right)\right] \tag{4}$$

where $V_s = 3\sqrt{3}l_p^2 t_0$ is the volume of the singum and t_0 the thickness when we look at the 2D lattice in the 3D space. For a 2D lattice with uniform material distribution in the thickness, we can write

$$t_0 = 1 \quad \text{and} \quad V_s = 3\sqrt{3}l_p^2 \tag{5}$$

which normalizes k in Eq. (3) through area A with a unit thickness. Here the thickness is fixed so that it is corresponding to a plane strain problem in physical testing, which can be straightforwardly extended to plane stress problems by mapping the elastic moduli (Yin and Zhao 2016). From Eq. (2), we obtain

$$V_{,r}|_{r=2l_p} = 2l_p k(1 - \lambda^0), \quad \text{and} \quad V_{,rr} = k \tag{6}$$

where $\lambda^0 = \frac{r_0}{2l_p}$ is the ratio of the free bond length r_0 to the framed bond length $2l_p$. Therefore, the stiffness in Eq. (4) is rewritten as

$$C_{ijkl} = \frac{k}{2\sqrt{3}}\left[\lambda^0\delta_{ij}\delta_{kl} + (4 - 3\lambda^0)(\delta_{ik}\delta_{jl} + \delta_{jk}\delta_{il})\right] \tag{7}$$

Here $\mathbf{C}$ changes with the expansion or contraction of the lattice through the variation of λ^0. From the stiffness tensor, we can derive all elastic constants.

Strictly speaking, the singum B or A is not a unit cell because neither of them can fill the 2D space by translation only. Mirror reflection or rotation of $\frac{\pi}{3}$ is needed to fill the space. However, the combination of the two of them forms a primitive cell, which can fill the space perfectly by translation only. Actually, the simplified singum model (Yin 2022) did not address the equilibrium of the node caused by the uniform virtual strain, which is not a problem for a primitive cell containing only a single node with central symmetry due to the periodicity of the forces. However, when a primitive cell contains two nodes, the interaction between the two nodes needs to be addressed.

Particularly, when α varies in the range from $\frac{2\pi}{3}$ toward $\frac{\pi}{3}$, if we still follow the above steps for singum modeling, two significant differences can be observed:

1. The singum A or B will not be a regular triangle anymore, and the singum changes from an equilateral triangle to an isosceles trapezoid.
2. Given a virtual displacement field in accordance with a uniform virtual strain field, the node in the center of the WS cell is subjected to 3 bonding forces. The resultant force on the node is not zero. The node needs to move to a new equilibrium position for the equilibrium, so a single singum may not be representative for the lattice.

To address these differences, we will find even for a regular honeycomb lattice, the resultant force by a uniform strain variation may not be zero either, which lead to a correction of the bond forces and an anisotropic stiffness instead. Two singums are required to balance the force as a primitive cell for the singum modeling, and their combination can represent the lattice deformation periodically.

Stress and strain of a singum for the stiffness prediction of a lattice

Although we questioned whether a single singum can represent the whole lattice in stiffness prediction, this subsection investigates the representativeness of a unit cell. Using the regular honeycomb lattice as an example, we have clarified the nodes A and B can form the smallest unit cell, namely primitive cell AB. Following the singum construction procedure, we can construct the singums for nodes A and B by using the Voronio decomposition in Fig. 2(a).

Consider the singums as continuum particles with stress transfer through their contact surfaces, and the resultant traction for each side should be equivalent to the force through the bonds cut by the surface. For the overall unit cell, we can see four surfaces with bond cutting. When the stress in the solid satisfies the equilibrium equation without any body force or inertia force, the stress integral of the cell can be written (Yin 2022)

$$S_{ij}^{cell} = \Sigma_{I=1}^{4} x_i^I F_j^I \tag{8}$$

where $\mathbf{x}^I$ indicates the coordinate of the I^{th} bond cutting point on the surface. Although the stress cannot be well-defined on each point in the singum, the volume average of the singum stress can be calculated from the above stress integral.

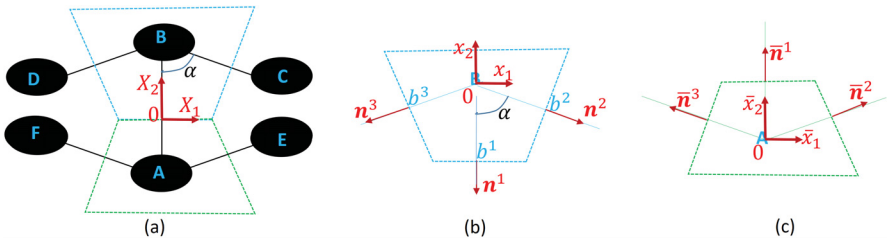

Fig. 2. The singum modeling of a unit cell containing two singums: (a) the overall unit cell containing two nodes A and B with four bonded nodes C, D, E, and F; (b) the singum B with its local coordinate, and (c) the singum A with its local coordinate

Notice that each node is required to be in equilibrium, and thus the overall equilibrium of the lattice can be guaranteed. However, an affine transformation of the lattice with a uniform strain may cause the loss of equilibrium of the nodes, particularly for Fig. 2(c). Therefore, the force calculated by the uniform strain field may not be the actual force for each bond, which should be carefully addressed. Before we move forward to singum modeling. We show five lemmas and one theorem about the definition of stress and strain, and the representativeness of the singum and unit cell of a lattice.

Lemma 1: When a singum contains a node with a force $\boldsymbol{b}^S(\boldsymbol{x}^S)$ *and N bond cutting points on the boundary with bonding forces* $\boldsymbol{F}^I(\boldsymbol{x}^I)$ $(I = 1, 2, \cdots, N)$*, which are in equilibrium with* $b_i^S + \Sigma_{I=1}^N F_i^I = 0$*, the stress integral in the corresponding space can be written as* $S_{ij}^S = x_i^S b_j^S + \Sigma_{I=1}^N x_i^I F_j^I$.

Proof: Conserve all forces of the lattice in the singum space. The forces in a continuum satisfy the equilibrium equation as

$$\sigma_{ij,i} + b_j^S \delta(\mathbf{x} \text{ - } \mathbf{x}^S) = 0 \tag{9}$$

where $\delta(\mathbf{x})$ is a Dirac Delta function. The boundary condition is written as

$$\sigma_{ij} n_i = \Sigma_{I=1}^N F_j^I \delta(\mathbf{x}\text{-}\mathbf{x}^I) \quad \text{for } \mathbf{x} \in \partial V_S \tag{10}$$

where V_S denotes the volume of the singum. The stress integral can be obtained by

$$S_{ij} = \int_{V_S} \sigma_{ij}(\mathbf{x}) d\mathbf{x} = \int_{\partial(V_S)} x_i \sigma_{kj} n_k d\mathbf{x} - \int_{V_S} x_i \sigma_{kj,k} x_j d\mathbf{x} = x_i^S b_j^S + \Sigma_{I=1}^N x_i^I F_j^I \tag{11}$$

The lemma is proved.

Lemma 2: When a singum contains N bond cutting points on the boundary with outward normal direction $\boldsymbol{n}^I$*, area* A^I*, and displacement* $\boldsymbol{u}^I$ *for the surface corresponding to the* I^{th} *cutting point, the strain integral in the singum can be written as* $E_{ij}^S = \Sigma_{I=1}^N \frac{A^I}{2} \left(u_i^I n_j^I + u_j^I n_i^I \right)$.

Proof: The strain in a continuum is defined by the compatibility of the displacement as

$$\varepsilon_{ij} = \frac{1}{2} \left(u_{i,j} + u_{j,i} \right) \tag{12}$$

The strain integral can be written as

$$E_{ij} = \int_{\partial V_S} \frac{1}{2}\left(u_i n_j + u_j n_i\right) dx = \Sigma_{I=1}^{N} \frac{A^I}{2}\left(u_i^I n_j^I + u_j^I n_i^I\right) \tag{13}$$

Because all points on one plane surface share the same $\mathbf{n}^I$ and the displacement integral can be represented by the central point, we can use the displacement at the bond cutting point to derive the surface integral. The lemma is proved.

Lemma 3: When a singum is in equilibrium under a set of forces on the node and bond cutting points, the average stress of a singum is independent from the translation of the Cartesian coordinate.

Proof: Provided a new coordinate $x_i' = a_i^0 + x_i$ with a_i^0 constant, we can obtain

$$S_{ij}' = \Sigma_{I=1}^{N}(x_i^I + a_i^0)F_i^I + x_i^b b_j = S_{ij} + a_i^0\left(\Sigma_{I=1}^{N} F_j^I + b_j\right) \tag{14}$$

where N denotes the number of bonds around the singum. Because $\Sigma_{I=1}^{N} F_j^I + b_j = 0$ for equilibrium, the second term is eliminated, and the lemma is proved.

With this lemma, although the origin of the coordinate does not make difference to the results, it is more convenient to set up the local coordinate with the origin at the node to simplify the calculation with $x_i^I = r n_i^I$.

Lemma 4: When two singums with $\boldsymbol{b}^1(\boldsymbol{X}^1) = -\boldsymbol{b}^2(\boldsymbol{X}^2)$, each of which is in equibrium, merge into a large cell, the stress integral over the large cell is equal to the sum of the stress integrals over the two singums and $\boldsymbol{b}^1(\boldsymbol{X}^1 - \boldsymbol{X}^2)$.

Proof: Consider two singums $\mathbf{S}$ and $\overline{\mathbf{S}}$ with their local coordinates related to each other at $\overline{x}_i = a_i^0 + x_i$ with $a_i^0 = X_i^2 - X_i^1$ being a constant. Based on *Lemma 2*, we can set up the local coordinates with the origin right on the nodes. The global coordinate $\mathbf{X}$ of the large cell can overlap with $\mathbf{x}$, the local coordinate of singum $\mathbf{S}$, without the loss of generality.

Their stress integrals of the two singums can be, respectively, written as

$$S_{ij} = \Sigma_{I=1}^{N} x_i^I F_j^I \quad \text{and} \quad \overline{S}_{ij} = \Sigma_{I=1}^{N} \overline{x}_i^I \overline{F}_j^I \tag{15}$$

where $\mathbf{x}^b = 0$ in the local coordinate is used. Assume that the contacted bond provides the forces in two singums, namely $\mathbf{F}^1$ and $\overline{\mathbf{F}}^1$ without the loss of generality. There are $2(N-1)$ boundary forces on the large cell with numbering from 2 to N on the two singums. The contacted forces and coordinates of the contacting point satisfy

$$\mathbf{F}^1 = -\overline{\mathbf{F}}^1 \quad \text{and} \quad \mathbf{x}^1 = \overline{\mathbf{x}}^1 - \mathbf{a}^0 \tag{16}$$

Using *Lemma 1*, we can write $\overline{S}_{ij}$ in the reference coordinate $\mathbf{x}$ as

$$\overline{S}_{ij} = \Sigma_{I=1}^{N}(\overline{x}_i^I - a_i^0)\overline{F}_j^I \tag{17}$$

Therefore, we can write the sum of stress integral referred to $\mathbf{x}$ as

$$S_{ij} + \overline{S}_{ij} = \Sigma_{I=1}^{N} x_i^I F_j^I + \Sigma_{I=1}^{N}(\overline{x}_i^I - a_i^0)\overline{F}_j^I \tag{18}$$

Using Eq. (16), $x_i^1 F_j^1 + (\overline{x}_i^1 - a_i^0)\overline{F}_j^1 = 0$, so that we can obtain

$$S_{ij} + \overline{S}_{ij} = \Sigma_{I=2}^{N} x_i^I F_j^I + \Sigma_{I=2}^{N} (\overline{x}_i^I - a_i^0)\overline{F}_j^I \tag{19}$$

For the large cell, using *Lemma 1*, we can write the stress integral as

$$S_{ij}^{cell} = \Sigma_{I=2}^{N} x_i^I F_j^I + \Sigma_{I=2}^{N} (\overline{x}_i^I - a_i^0)\overline{F}_j^I + X_i^1 b_j^1 + X_i^2 b_j^2 \tag{20}$$

Because $X_i^1 b_j^1 + X_i^2 b_j^2 = \left(X_i^1 - X_i^2\right) b_j^1$, the lemma is proved.

When primitive cells merge together, because of the repetivity of the unit cells and the equilibrium of each node, the last term of Eq. (20) disappear, so that the stress integral over the large cell is simply equal to the sum of those over the singums.

In general, unit cells can be set up with a node split by multiple unit cells when it is on the unit cell boundary or surface. Although we could deal with a boundary node by weighting the force cautiously, for simplicity and clarity of derivation, we define that a unit cell consisting the combination of WS cells as the WS unit cell to differentiate it from general unit cells with boundary nodes. The primitive cell in Fig. 2(a) with two nodes is the smallest WS unit cell.

Lemma 5: When two WS unit cells merge into a large cell, the stiffness of the large cell is equal to the stiffness of the WS unit cell.

Proof: The stiffness of the lattice can be derived by applying a displacement variation in accordance with a uniform strain on the boundary of the unit cell, which satisfies the periodic boundary conditions and the equilibrium condition inside. Although each node may move in the unit cell to reach the equilibrium position, the bonding forces on the boundary are periodic and their resultant force will be in equilibrium as well. Because the nodes are in equilibrium, using *Lemma 4*, we can see the stress integral over the large cell is simply the combination of the stress integral over each WS cell. Therefore, the large cell and small cells will exhibit the same average stress, which leads to the same stiffness of the large cell as the small WS cell. The lemma is proved.

As there are many ways to form unit cells, the uniqueness of the stiffness among unit cells is important. Although a WS primitive cell can represent all WS cells for the stiffness prediction, the following theorem can be significant for general unit cells.

Theorem 1: When the short-range interactions between the nodes are considered, the stiffness of a unit cell of a crystal lattice is independent from the unit cell shape or size.

Proof: Consider a unit cell $\mathbf{U}$ including M nodes, in which N nodes exhibit surface bonds across the boundary of the unit cell. Therefore $M \geq N$. Using the M nodes, we can form another unit cell $\overline{\mathbf{U}}$ with a combination of WS primitive cells as well, which exhibit the same stiffness as the stiffness of a single WS primitive cell based on *Lemma 5*. However, the surface bond cutting point in the general unit cell $\mathbf{U}$ may not be the same as the WS unit cell $\overline{\mathbf{U}}$, which leads to different numerical expression for each term of $x_i^I F_j^I$ $(I = 1, 2, ..., N)$ because of different x_i^I. However, we can use either $\mathbf{U}$ or $\overline{\mathbf{U}}$ to fill the lattice space.

Now assume that there is a difference of the stiffness between $\mathbf{U}$ and $\overline{\mathbf{U}}$. Under a uniform strain, the stress integral over $\mathbf{U}$ and $\overline{\mathbf{U}}$ will be different. Considering the

periodicity of unit cells, we can pack a 3D volume of the lattice with L cells in each dimension by two types of the unit cells, respectively, the difference of stress integral increases with the surface area at a scale L^2, but the volume increases at a scale L^3, because the surface area cannot proportionally increase with the volume due to merging the surface nodes with N surface bonds. From Eq. (4) we can see the difference of the stiffness for the 3D volume packed by the two types of unit cells always converges to zero. However, based on *Lemma 4*, the stress integrals proportionally increase with the volume for both unit cell cases, so the stiffness of the 3D volume for the two cases will remain the same with the increase of L. Therefore, the initial assumption cannot be true, so that the stiffness of $\mathbf{U}$ must be the same as $\overline{\mathbf{U}}$, which is a constant. When a general unit cell has atoms on the cell's boundary, we can split the integral among the neighboring unit cells cautiously with an appropriate weight, which will be merged with volume increase and thus obtain the same conclusion. The theorem is proved.

Singum modeling of a primitive cell containing two singums

Now we start the singum modeling for the primitive cell in Fig. 2(a). When the lattice is subjected to a uniform loading, the deformed lattice will still exhibit a repetitive pattern shown by unit cells. If each bond deforms in the same pattern, the bond force can be obtained. As reviewed in the last subsection, the simplified singum model assumed the displacement variation corresponding to a uniform strain variation is applicable to every point in the lattice (Yin 2022). It is a strong assumption but may cause equilibrium issues.

Use singum B in Fig. 2(b) as an example. When a displacement variation is applied to the cell as $\delta u_i(\mathbf{x}) = \delta\varepsilon_{ij}x_j$, which is corresponding to a uniform strain variation of $\delta\varepsilon_{ij}$ at every point in the cell. It produces an infinitesimal change of the forces on each bond as:

$$\delta F_i^I = \frac{d(F_i^I)}{dx_k}\delta u_k = (2l_pV_{,rr}^I - V_{,r}^I)n_i^I n_k^I n_l^I \delta\varepsilon_{kl} + V_{,r}^I n_k^I \delta\varepsilon_{ki} \tag{21}$$

where $\mathbf{n}$ can be seen from Figs. 2(b). Then, we can write $\mathbf{n}^1 = (0,-1)$,$\mathbf{n}^2 = (\sin\alpha, -\cos\alpha)$, and $\mathbf{n}^3 = (-\sin\alpha, -\cos\alpha)$ in Fig. 2(b). Because we use the bonds with the same bond length, all bonds share the same derivatives of $V_{,r}$, so the superscript of "I" is only needed for the direction norm $\mathbf{n}^I$ of the bonds. The resultant force caused by the three bonds can be written as

$$\delta P_i^B = \Sigma_{I=1}^3 \delta F_i^I = \Sigma_{I=1}^3 \left[(2l_pV_{,rr} - V_{,r})n_i^I n_k^I n_l^I + V_{,r}n_k^I\delta_{il}\right]\delta\varepsilon_{kl} \tag{22}$$

In the same fashion, another resultant force on singum A also exists, written as δP_i^A. Due to the equilibrium or the central symmetry of singums A and B referred to the mid-point of AB, we can obtain $\delta P_i^B = -\delta P_i^A$.

These forces will cause the nodes A and B to move with central symmetry to the mid-point of AB and the forces will be redistributed among the bonds for equilibrium. As long as the displacement variations of the four bond-cutting points satisfy the periodic boundary condition corresponding to a uniform strain $\delta\varepsilon_{ij}$, based on *Lemma 2*, the average strain variation on the primitive cell will be the same as $\delta\varepsilon_{ij}$.

The actual solution of the forces can be the superposition of the two cases:
Case I: A uniform displacement field in the whole unit cell with the two external forces

($-\delta\mathbf{P}^B$ and $-\delta\mathbf{P}^A$) applied, which will satisfy the equilibrium for both nodes and uniform lattice variation.
Case II: The bond cutting points of the unit cell is fixed, and two inverse forces ($\delta\mathbf{P}^B$ and $\delta\mathbf{P}^A$) are applied on B and A, respectively.
The superposition of the two cases makes both the periodic boundary condition of the unit cell and the equilibrium condition of the nodes satisfied, and thus recovers the original problem. For Case I, based on *Lemma 4*, the stress integral over the primitive cell can be written as

$$\delta S_{ij}^{AB} = \delta S_{ij}^{A} + \delta S_{ij}^{B} - \delta P_i^B (X_j^B - X_j^A) \tag{23}$$

Using *Lemma 3*, we can move the local coordinate origin to node B as shown in Fig. 2(b) and number the bond AB as 1 in each singum. Using *Lemma 1*, we can write $\delta S_{ij}^{B} = \Sigma_{I=1}^{3} x_i^I \delta F_j^I - x_i^B \delta P_j^B = \Sigma_{I=1}^{3} x_i^I \delta F_j^I$.

The singum A can be conducted in the same fashion with the local coordinate $\overline{\mathbf{x}}$ in Fig. 2(c) as $\delta S_{ij}^{A} = \Sigma_{I=1}^{3} \overline{x}_i^I \delta \overline{F}_j^I$.

For Case II, based on *Lemma 4*, the stress integral can be written as

$$\delta S_{ij}^{AB} = \delta S_{ij}^{A} + \delta S_{ij}^{B} + (X_i^B - X_i^A) \delta P_j^B \tag{24}$$

Due to the symmetry, the mid-point of AB shall not move as well when the four bond cutting points are fixed and two opposite forces are applied at Nodes A and B, respectively. Now focus on Singum B. The unbalanced force $\delta\mathbf{P}^B$ should be redistributed among the three bonds so that we can derive S_{ij}^B. Because there are three bonds to balance one force, the compatibility of the bond deformation shall be used in general. We can calculate the redistributed force on each bond by a static analysis.

Given a unit force $\mathbf{f} = 1$ applied to node B in x_i direction, the force will distribute among three bonds. We define the ratio of the distributed force on bond I caused by a unit force x_i on B as R_i^I, which forms a constant matrix depending on the geometry of the lattice and will be demonstrated in the next section. Therefore, if a force is written in terms of $\mathbf{F} = F_i \mathbf{e}_i$ on the node, the distributed forces are on the I^{th} bond can be written $R_i^I F_i \mathbf{n}^I$. Following this fashion, the bond force variation for bond I is written as $\delta\mathbf{T}^I$:

$$\delta T_j^I = \Sigma_{J=1}^{3} \left[(2 l_p V_{,rr} - V_{,r}) R_m^I n_m^J n_k^J n_l^J + V_{,r} R_l^I n_k^J \right] n_j^I \delta\varepsilon_{kl} \tag{25}$$

Therefore, the stress integral for Case II can be obtained $\delta S_{ij}^{B} = \Sigma_{I=1}^{3} x_i^I \delta T_j^I$.

The total stress integral of singum B for combining two cases is obtained as

$$\delta S_{ij}^{B} = \Sigma_{I=1}^{3} x_i^I (\delta F_j^I + \delta T_j^I) \tag{26}$$

Although $\mathbf{F}^I$ and $\mathbf{T}^I$ was assumed to be zero at the initial condition, for consistence with the general case (Yin 2022), if prestress exists, we can also write $\mathbf{F}^I = V_{,r} \mathbf{n}^I$, but $\mathbf{T}^I = 0$ due to the equilibrium.

The stiffness tensor C_{ijkl} of the singum B can be obtained by the average stress variation over the singum B as

$$\begin{aligned}\delta\sigma_{ij}^{B} &= \Sigma_{I=1}^{3}\left[\frac{x_i^I(\delta F_j^I+\delta T_j^I)}{V_s/2}+\frac{x_k^I F_j^I\delta\varepsilon_{ki}}{V_s/2}-\frac{x_i^I F_j^I\delta\varepsilon_{kk}}{V_s/2}\right]\\ &= \frac{2l_p}{V_s/2}\Sigma_{I=1}^{3}\left[(\delta F_j^I+\delta T_j^I)n_i^I+F_j^J\delta_{il}\delta\varepsilon_{kl}n_l^I-F_j^J n_i^I\delta\varepsilon_{kk}\right]\\ &= \frac{2}{V_s}\Sigma_{I=1}^{3}\left[(4V_{,rr}l_p^2-2V_{,r}l_p)n_i^I n_j^I n_k^I n_l^I+2V_{,r}l_p(\delta_{il}n_j^I n_k^I+\delta_{jl}n_i^I n_k^I-\delta_{kl}n_i^I n_j^I)\right]\delta\varepsilon_{kl}\\ &+ \frac{2}{V_s}\Sigma_{I=1}^{3}\Sigma_{J=1}^{3}\left[(4V_{,rr}l_p^2-2V_{,r}l_p)R_m^I n_m^J n_k^J n_l^J n_i^I n_j^I+2V_{,r}l_p R_l^I n_k^J n_i^I n_j^I\right]\delta\varepsilon_{kl}\end{aligned} \tag{27}$$

where $V_s = 8l_p^2\sin\alpha(1-\cos\alpha)$ with the unit thickness. Here only a half of V_s is taken for singum B. Define two tensors as

$$\begin{aligned}E_{ijkl}^1 &= \Sigma_{I=1}^{3}(\delta_{il}n_j^I n_k^I+\delta_{jl}n_i^I n_k^I-\delta_{kl}n_i^I n_j^I)+\Sigma_{I=1}^{3}\Sigma_{J=1}^{3}R_l^I n_k^J n_i^I n_j^I\\ E_{ijkl}^2 &= \Sigma_{I=1}^{3}n_i^I n_j^I n_k^I n_l^I+\Sigma_{I=1}^{3}\Sigma_{J=1}^{3}R_m^I n_m^J n_k^J n_l^J n_i^I n_j^I\end{aligned} \tag{28}$$

we can rewrite Eq. (27) as

$$\delta\sigma_{ij} = \frac{2}{V_s}\left[2V_{,r}l_p E_{ijkl}^1+(4V_{,rr}l_p^2-2V_{,r}l_p)E_{ijkl}^2\right]\delta\varepsilon_{kl} \tag{29}$$

The same procedure can be done for singum A, where we can define $\overline{\mathbf{n}}^1 = (0,1)$, $\overline{\mathbf{n}}^2 = (\sin\alpha,\cos\alpha)$, and $\overline{\mathbf{n}}^3 = (-\sin\alpha,\cos\alpha)$ in Fig. 2(c). The stiffness tensor of the singum can be obtained from the above relationship between the averaged virtual stress and strain over the singum as follows:

$$C_{ijkl} = \frac{1}{V_s}\left[2V_{,r}l_p(E_{ijkl}^1+\overline{E}_{ijkl}^1)+(4V_{,rr}l_p^2-2V_{,r}l_p)(E_{ijkl}^2+\overline{E}_{ijkl}^2)\right] \tag{30}$$

where $\overline{\mathbf{E}}^1$ and $\overline{\mathbf{E}}^2$ are the counterparts of $\mathbf{E}^1$ and $\mathbf{E}^2$ in singum A.

The above derivation procedure is general and can be extended to other types of lattices, including 3D lattice as well. Notice that the overall stiffness in Eq. (30) will be different but more accurate than Eq. (7) when $\alpha = \frac{2\pi}{3}$.

RESULTS AND DISCUSSION

Given the characteristics of a lattice including the geometry, elastic potential of the bonds, and prestress of the bonds, we can derive the effective elasticity $\mathbf{C}$ in Eqs. (4) and (30). Note that the first one did not consider the equilibrium and is not physical, so that the latter formulation should be used for the physical soundness and accuracy.

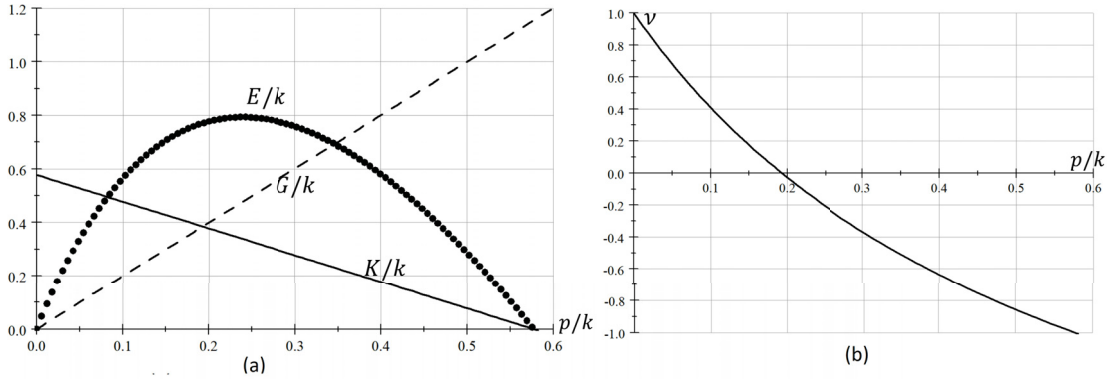

Fig. 3. The elastic constants versus the pre-stress p/k for the regular honeycomb lattice: (a) the normalized elastic moduli and (b)the Poisson's ratio

Elasticity variation with prestress in a regular honeycomb lattice

When a regular honeycomb lattice with the linear elastic potential of bonds is subjected to a uniform biaxial loading $\sigma_{ij} = p\delta_{ij}$ in the 2D plane, which is also a hydrostatic stress in 2D, from Fig. 1(a), the force in the bond F is related to p or bond length $2l_p$ as follows:

$$F = 2\sqrt{3}l_p p = k(2l_p - r_0) \quad \text{or} \quad \lambda^0 = 1 - \sqrt{3}\frac{p}{k} \tag{31}$$

In Fig. 2(b) with $\alpha = \frac{2\pi}{3}$, we can obtain $\mathbf{n}^1 = (0, -1)$,$\mathbf{n}^2 = (0.866, 0.5)$, and $\mathbf{n}^3 = (-0.866, 0.5)$. Given a displacement variation over the lattice corresponding to the uniform strain variation, Eq. (32) will show a resultant force on B because the three bonds are in the different orientation. For example,when a uniform strain $\Delta\varepsilon_{11} = e_0$ is applied, the resultant force on B will be

$$\Delta P_1^B = 0 \quad \text{and} \quad \Delta P_2^B = \frac{3e_0}{4}(2l_p V_{,rr} - V_{,r}) \tag{32}$$

This unbalanced force is redistributed to the bonds through the redistribution matrix as $R_i^I P_i^B$ with

$$R_i^I = \begin{pmatrix} 0 & \frac{2}{3} \\ -\frac{\sqrt{3}}{3} & -\frac{1}{3} \\ \frac{\sqrt{3}}{3} & -\frac{1}{3} \end{pmatrix} \tag{33}$$

which is obtained by the static analysis with a unit force on x_1 or x_2, respectively. Therefore, bond 1 will show tension force and bonds 2 and 3 compression from the redistribution of the force, which will affect the average stress and the stiffness as well. However, when a primitive cell contains a single node, the bonds can be paired due to the periodicity with each $\mathbf{n}^I$ matching with $-\mathbf{n}^I$ for another bond, and the resultant force is always zero. As a result, no force redistribution is required and the simplified singum model will provide accurate results for single-node primitive cells.

Using Eq. (33) in Eq. (28), we can write $\mathbf{E}^1$ and $\mathbf{E}^2$ in the Voight notation as follows:

$$E_{IJ} = \begin{pmatrix} E_{1111} & E_{1122} & E_{1112} \\ E_{2211} & E_{2222} & E_{2212} \\ E_{1211} & E_{1222} & E_{1212} \end{pmatrix} \tag{34}$$

where the mapping of $ij \rightarrow I$ is set up as $11 \rightarrow 1$, $22 \rightarrow 2$, $12 \rightarrow 3$, which can be applied to both stress and strain as well. We can obtain

$$E^1_{IJ} = \begin{pmatrix} 1.5 & -1.5 & 0 \\ -1.5 & 1.5 & 0 \\ 0 & 0 & 1.5 \end{pmatrix} \tag{35}$$

and

$$E^2_{IJ} = \begin{pmatrix} 0.75 & 0.75 & 0 \\ 0.75 & 0.75 & 0 \\ 0 & 0 & 0 \end{pmatrix} \tag{36}$$

Actually, the singum A exhibits the same tensors as the above, so that the effective stiffness of the lattice can be written by the substitution of the above two tensors into Eq. (30) as

$$C_{IJ} = \frac{8kl_p^2}{V_s}\left[(1-\lambda^0)\begin{pmatrix} 1.5 & -1.5 & 0 \\ -1.5 & 1.5 & 0 \\ 0 & 0 & 1.5 \end{pmatrix} + \lambda^0 \begin{pmatrix} 0.75 & 0.75 & 0 \\ 0.75 & 0.75 & 0 \\ 0 & 0 & 0 \end{pmatrix}\right] \tag{37}$$

Using the relationship of Eq. (31), we can write the stiffness tensor in terms of the prestress p as well:

$$C_{IJ} = \frac{\sqrt{3}k}{3}\begin{pmatrix} 1+\sqrt{3}\frac{p}{k} & 1-3\sqrt{3}\frac{p}{k} & 0 \\ 1-3\sqrt{3}\frac{p}{k} & 1+\sqrt{3}\frac{p}{k} & 0 \\ 0 & 0 & 2\sqrt{3}\frac{p}{k} \end{pmatrix} \tag{38}$$

Using a biaxial loading for pure shearing and hydrostatic tests in the 2D plane, we can write the shear modulus and bulk modulus as:

$$\frac{K}{k} = \frac{1}{\sqrt{3}}\left(1-\sqrt{3}\frac{p}{k}\right); \quad \frac{G}{k} = 2\frac{p}{k} \tag{39}$$

Using a unit uniaxial loading test with $\sigma_{11} = 1, \sigma_{22} = \sigma_{12} = 0$, we can solve for ε_{ij} and write the Young's modulus and Poisson's ratio as

$$\frac{E}{k} = \frac{1}{\varepsilon_{11}} = 8\frac{(1-\sqrt{3}\frac{p}{k})\frac{p}{k}}{1+\sqrt{3}\frac{p}{k}}; \quad \nu = -\frac{\varepsilon_{22}}{\varepsilon_{11}} = \frac{1-3\sqrt{3}\frac{p}{k}}{1+\sqrt{3}\frac{p}{k}} \tag{40}$$

Fig. 3 shows the elastic constants changing with the normalized prestress p/k. Although the bonds follows linear elastic behavior, the effective elastic moduli in Fig. 3(a) are not constant for the lattice but change quickly with the prestress, which exhibits the following features:

1. When $p/k = 0$, both the shear modulus and Young's modulus is zero, and increases rapidly with p/k.
2. Both the shear modulus and bulk modulus linearly change with p, but the bulk modulus decreases with a slope of "-1" whereas the shear modulus increase with a slope of "2".
3. The Young's modulus increases to a peak point at $p/k = 0.239$ (or $\frac{\sqrt{2}}{\sqrt{3}} - \frac{1}{\sqrt{3}}$), and then decreases to zero at $p/k = \sqrt{3}/3$, where the bulk modulus is zero as well.
The decrease of bulk modulus with p to zero at $p/k = 0.577$ (or $\sqrt{3}/3$) is caused by the configurational force during the variation of the average stress as follows: given a tensile stress vector $\mathbf{p}^0$ on the boundary of singum B in Fig. 1(a), the circumference of the singum increases to a certain value A^0 and the force on one bond is $\mathbf{P}^0 A^0/3$ at the equilibrium. When a small increase of area ΔA is applied, a small bond force change ΔF will be caused by the bond length increment. Even without changing the tensile stress vector, $\mathbf{p}^0$ will produce a larger force to the bond at $\mathbf{p}^0 \Delta A$. If it is balanced by ΔF, it means no stress is needed to cause the expansion, the lattice will lose the stability unless the stress vector reduces. Therefore it is physical and reasonable to have the bulk modulus reducing to zero and then lose the stability because the bond force cannot sustain the force generated in 2D surface.

The instability problem at $p = 0$ is different from the case of $p/k = 0.577$. From the projection of the curve, when $p < 0$, the shear modulus will become negative which shows the loss of stability. Consider the red rectangular unit cell in Fig. 1(a). A pressure $\mathbf{p}^0$ is applied on each side as a prestress. When a small elongation is applied along AB, at the prependicular direction to AB, a larger surface force will be caused, which leads to shearing instability. Although the lattice can sustain high hydrostatic pressure, it is not stable as the shape of the lattice can easily be distorted by the shear strain. Therefore, the stable prestress range of p/k should be in $(0, 0.577)$.

Fig. 3(b) shows the Poisson's ratio. When $p = 0$, the Poisson's ratio is 1, which is beyond the normal range of the Poisson's ratio of (-1,0.5) in 3D problems. For regular isotropic elastic solids, the Poisson's ratio in a 2D plane strain problem can be related to the 3D counterpart by $\nu^{3D} = \frac{\nu}{1+\nu}$. In 3D problem, the Poisson's ratio is in the range of (-1,0.5), but in the 2D plane strain problem, the Poisson's ratio can be calculated in the range of $(-\infty, 1)$ instead. When $\frac{p}{k} > \frac{1}{3\sqrt{3}}$ or $\lambda^0 < \frac{2}{3}$, the Poisson's ratio becomes negative.

By changing the characteristic angle α to $(\pi/3,\pi/2)$ in Fig. 2, we can demonstrate the auxetic metamaterial without the necessity of prestress.

Demonstration of the effective elasticity of the 2D auxetic metamaterial

Eq. (30) provides a concise form of the stiffness tensor of the primitive cell AB, which can represent the overall stiffness based on **Theorem 1**. For simplicity and clarity, we choose the case of $\alpha = \pi/3$ to demonstrate the procedure to use the formulation, which can be extended to other cases of α or other types of auxetic metamaterials based on different lattices. In addition, this section assumes the prestress is zero although it can be extended to the case with prestress in the same fashion of the last subsection.

In Fig. 2(a), although D and F, or C and E, will overlap with each other at $\alpha = \pi/3$, we do not allow them to link with each other, so that they can separate freely. Actually,

it is feasible to have $\alpha < \pi/3$ if we allow the bond to overlap with each other but not have force contact. However, it is not clear to show it visually with an ill-conditioned lattice. This paper avoids it.

As we have seen in the last section, the effective elasticity depends on k and prestress. Here the prestress is set at 0. The bond length does not change the effective elasticity numerically, so we use the normalized length at 1. Given $\alpha = \pi/3$, we obtain

$$V_s = 8l_p^2 \sin\alpha(1 - \cos\alpha) = 2\sqrt{3} \tag{41}$$

Using the geometry in Fig. 2(b), we can obtain $\mathbf{n}^1 = (0, -1)$, $\mathbf{n}^2 = (0.866, -0.5)$, and $\mathbf{n}^3 = (-0.866, -0.5)$. The redistribution matrix of R_i^I can be obtained by the static analysis with a unit force on x_1 or x_2, respectively, which is written

$$R_i^I = \begin{pmatrix} 0 & \frac{2}{3} \\ -\frac{\sqrt{3}}{3} & \frac{1}{3} \\ \frac{\sqrt{3}}{3} & \frac{1}{3} \end{pmatrix} \tag{42}$$

which is obtained by the static analysis. The force transfer in the lattice is significantly different from the regular honeycomb lattice, which causes the average stress to not be a symmetric tensor anymore, namely $\sigma_{12} \neq \sigma_{21}$ under a uniform shear strain on the lattice. Physically, a uniform shear strain cannot be naturally achieved by uniform stresses, and an external moment is required to balance the torque. Therefore, the traditional Voight notation will not be sufficient for E_{IJ}^1. We can write

$$E_{IJ}^1 = \begin{pmatrix} 1.5 & -1.5 & 0 \\ -2.5 & -0.1667 & 0 \\ 0 & 0 & 0.5 \\ 0 & 0 & 0 \end{pmatrix} \tag{43}$$

and

$$E_{IJ}^2 = \begin{pmatrix} 0.75 & -0.25 & 0 \\ -0.25 & 0.0833 & 0 \\ 0 & 0 & 0 \end{pmatrix} \tag{44}$$

where in Eq. (43), the fourth row means σ_{21} caused by three strain components as zero, which is different from the third row of σ_{12}. For regular honeycomb lattices, this problem does not exist as $\Sigma_{J=1}^3 n_i^J = 0$. This issue shall be further investigated in the future work.

As the auxetic metamaterials are mainly subjected to normal stress for the benefits of the negative Poisson's ratio, we can focus on the components of $I, J = 1, 2$ instead. Actually, the singum A exhibits the same tensors as the above, so that the effective stiffness of the lattice can be written by the substitution of the above two tensors into Eq. (30) as

$$C_{IJ} = \frac{8kl_p^2}{V_s}\left[(1 - \lambda^0)\begin{pmatrix} 1.5 & -1.5 \\ -2.5 & -0.1667 \end{pmatrix} + \lambda^0 \begin{pmatrix} 0.75 & -0.25 \\ -0.25 & 0.0833 \end{pmatrix}\right] \tag{45}$$

Now without any prestress, $\lambda^0 = 1$, so the above equation is simplified as

$$C_{IJ} = \frac{4k}{\sqrt{3}} \begin{pmatrix} 0.75 & -0.25 \\ -0.25 & 0.0833 \end{pmatrix} \tag{46}$$

Using the above relationship, we can see for the lattice with $\alpha = \pi/3$:
1. Given an uniaxial loading in x_1 direction, the Young's modulus is zero and the Poisson's ratio is -3 for $\alpha = \pi/3$;
2. Given an uniaxial loading in x_2 direction, the Young's modulus is still zero but the Poisson's ratio becomes $-1/3$.
3. Although the lattice shows zero stress when $\varepsilon_{11} : \varepsilon_{22} = 1 : 3$, the lattice still exhibits stiffness for the displacement controlled test at other modes.

For example, given a uniaxial elongation with $\varepsilon_{11} = a; \varepsilon_{22} = 0$, the load of $4ka/\sqrt{3}\,(0.75, -0.25)$ is required; whereas given a uniaxial elongation with $\varepsilon_{22} = a$, the load of $4ka/\sqrt{3}\,(-0.25, 0.08335)$ is required. Obviously, the material exhibits different stiffness in the two directions with an anisotropic behavior. The formulation can be used for designs of metamaterials by changing the bond lengths and α of lattices .

Demonstration of the effective elasticity of the body-centered cubic (BCC) lattice

Body center cubic (BCC) lattices exist in many materials and composites, such as the crytal structure of metals (Weinberger et al. 2013), macromolecular chain structure (Arruda and Boyce 1993), carbon nanotube network (Jang and Yin 2015), fiber micro-lattice composites (Xiong et al. 2015), and periodic particulate composites (Yin et al. 2002), which exhibit different types of potential functions of the bonds. Although various constitutive modeling methods existed in the literature to simulate the material behavior for specific loading conditions, an explicit form of the stiffness tensor for BCC lattice is particularly useful for the material design and analysis. The singum model can serve this purpose very well.

Following the last section, we still use the elastic potential for the bonds in Eq. (2) to construct the singum model and predict the effective elasticity of the lattice. The 2D singum model can be straightforwardly extended to 3D for general crystal lattice in the same fashion. Here we focus on the BCC lattice in Fig. 4 as an example, which can be generalized to face-centered cubic (BCC) and simple cubic (SC) lattices as well. Fig. 4 shows the unit cell of a BCC lattice with the cubic edge length a, so that the bond length $2l_p = \frac{\sqrt{3}a}{2}$. We set up the coordinate with the origin at the 0^{th} atom, and 8 closest neighbor atoms are located at $(\pm\frac{a}{2}, \pm\frac{a}{2}, \pm\frac{a}{2})$, which are corresponding to the directional vectors $\mathbf{n}^I$ $(I = 1, 2, ..., 8) = (\pm\frac{1}{\sqrt{3}}, \pm\frac{1}{\sqrt{3}}, \pm\frac{1}{\sqrt{3}})$.

Following the same procedure as the 2D case, for each bond between the 0^{th} atom at the center of the front surface and the 8 member atoms, we can use a perpendicular plane ABC to cut the bond at the midpoint as shown in Fig. 4 for the bond of atom pair 0-1, which shall be repeated for other 7 pairs within in the cube. Eventually, we can obtain the BCC singum as a truncated octahedron. The volume of the singum can be written as

$$V_s = \frac{a^3}{2} = \frac{32\sqrt{3}l_p^3}{9} \tag{47}$$

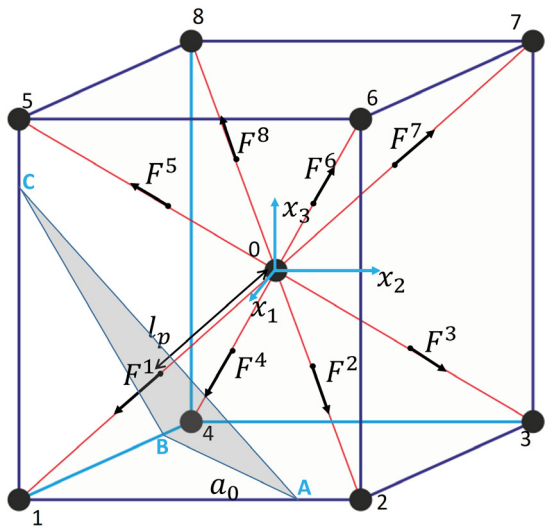

Fig. 4. The unit cells for the singum model construction at Atom 0 of a body centered cubic lattice with 8 members

Because the primitive cell of BCC contains one node only, the node will always stay in equilibrium under a displacement variation corresponding to a uniform strain and no force redistribution is needed. The following identities for normal vectors in the 3D space will be used for stiffness prediction:

$$\begin{aligned}
&\Sigma_{I=1}^{8} n_i^I n_j^I = \frac{8}{3}\delta_{ij} \\
&\Sigma_{I=1}^{8} n_i^I n_j^I n_k^I n_l^I = \frac{8}{9}\left[(1-2\delta_{IK})\delta_{ij}\delta_{kl} + (\delta_{ik}\delta_{jl} + \delta_{jk}\delta_{il})\right]
\end{aligned} \tag{48}$$

When the terms with subscript indices including both uppercase and lowercase letters, Mura's extended index notation is used as follows (Mura 1987; Yin and Zhao 2016):

1. Repeated lower case indices are summed up as usual index notation;
2. Uppercase indices take on the same numbers as the corresponding lower case ones, but are not summed.

Similarly to Eq. (27), one can rewrite it by using Eq. (48) instead as

$$\begin{aligned}
\delta\sigma_{ij} &= \Sigma_{I=1}^{8}\left[\frac{x_i^I \delta F_j^I}{V_s} + \frac{x_k^I F_j^I \delta\varepsilon_{ki}}{V_s} - \frac{x_i^I F_j^I \delta\varepsilon_{kk}}{V_s}\right] \\
&= \frac{1}{V_s}\Sigma_{I=1}^{8}\left[(4V_{,rr}l_p^2 - 2V_{,r}l_p)n_i^I n_j^I n_k^I n_l^I + 2V_{,r}l_p(\delta_{il}n_k^I n_j^I + \delta_{jl}n_i^I n_k^I - \delta_{kl}n_i^I n_j^I)\right]\delta\varepsilon_{kl} \\
&= \frac{32}{9V_s}\left[\left(V_{,rr}l_p^2 - 2V_{,r}l_p - (2V_{,rr}l_p^2 - V_{,r}l_p)\delta_{IK}\right)\delta_{ij}\delta_{kl} + (V_{,rr}l_p^2 + V_{,r}l_p)(\delta_{ik}\delta_{jl} + \delta_{il}\delta_{jk})\right]\delta\varepsilon_{kl}
\end{aligned} \tag{49}$$

The stiffness tensor of the singum can be obtained from the above relationship between

the averaged virutal stress and strain over the singum as follows:

$$C_{ijkl} = \frac{32}{9V_s}\left[\left(V_{,rr}l_p^2 - 2V_{,r}l_p - (2V_{,rr}l_p^2 - V_{,r}l_p)\delta_{IK}\right)\delta_{ij}\delta_{kl} + (V_{,rr}l_p^2 + V_{,r}l_p)(\delta_{ik}\delta_{jl} + \delta_{il}\delta_{jk})\right] \tag{50}$$

Using the Voight's notation, we can obtain the three elastic constants for the cubic symmetric stiffness tensor as

$$C_{11} = \frac{32}{9V_s}\left(V_{,rr}l_p^2 + V_{,r}l_p\right); \quad C_{12} = \frac{32}{9V_s}\left(V_{,rr}l_p^2 - 2V_{,r}l_p\right); \quad C_{44} = \frac{32}{9V_s}\left(V_{,rr}l_p^2 + V_{,r}l_p\right) \tag{51}$$

Using Eq. (6), we can rewrite the above equation as

$$C_{11} = \frac{k}{\sqrt{3}l_p}\left(3 - 2\lambda^0\right); \quad C_{12} = \frac{k}{\sqrt{3}l_p}\left(-1 + 2\lambda^0\right); \quad C_{44} = \frac{k}{\sqrt{3}l_p}\left(3 - 2\lambda^0\right) \tag{52}$$

When no prestress is applied as $\lambda^0 = 1$, we can obtain $C_{11} = C_{12} = C_{44} = \frac{k}{\sqrt{3}l_p}$, which shows that a uniaxial elongation will produce the same stress in all directions due to the central symmetry and each node shared by three surfaces in the unit cell. Although all these elastic moduli are positive, because they are not linearly independent, the BCC lattice may not produce stress for some deformation mode corresponding to $\varepsilon_{11} + \varepsilon_{22} + \varepsilon_{33} = 0$ in the infinitesimal strain state, which causes the rotation of bonds or octahedral shear strain. The lattice can sustain the hydrostatic load $\varepsilon_{11} = \varepsilon_{22} = \varepsilon_{33} = p$ with a bulk modulus at $k = \frac{k}{\sqrt{3}l_p}$ as well.

Although the lattice shows a zero stress for some strain mode at the infinitesimal strain state, it does not mean the lattice will surely lose the stability, because the elastic constants changes with the prestress or λ^0 as well. When a prestress exists, similarly to the case of the regular honeycomb lattice, the shear modulus can be nonzero which will be discussed subsequently. When the orientation of the lattice changes, stress can be developed among the lattice and resist the deformation with the cubic symmetry of the stiffness. In addition, when the unit cells of the lattice are not perfectly repeated, and some randomness is introduced for the connection between the unit cells, the shear resistance can be developed by bonds as well. The randomly connected unit cells form an isotropic volume statistically. We can use the orientational average of the cubic symmetric stiffness to estimate the bulk modulus and shear modulus as

$$\frac{K}{k} = \frac{C_{11} + 2C_{12}}{3k} = \frac{1 + 2\lambda^0}{3\sqrt{3}l_p}; \quad \frac{\mu}{k} = \frac{C_{11} - C_{12} + 3C_{44}}{5k} = \frac{13 - 10\lambda^0}{5\sqrt{3}l_p} \tag{53}$$

from which, we can derive the Young's modulus and Poisson's ratio as

$$\frac{E}{k} = \frac{(1 + 2\lambda^0)(13 - 10\lambda^0)}{6\sqrt{3}l_p}; \quad \nu = \frac{-7 + 10\lambda^0}{12} \tag{54}$$

Fig. 5 shows the normalized elastic constants by a factor of l_p/k changing with the bond length ratio $\lambda^0 = r^0/(2l_p)$. Although the bonds follows linear elastic behavior, the

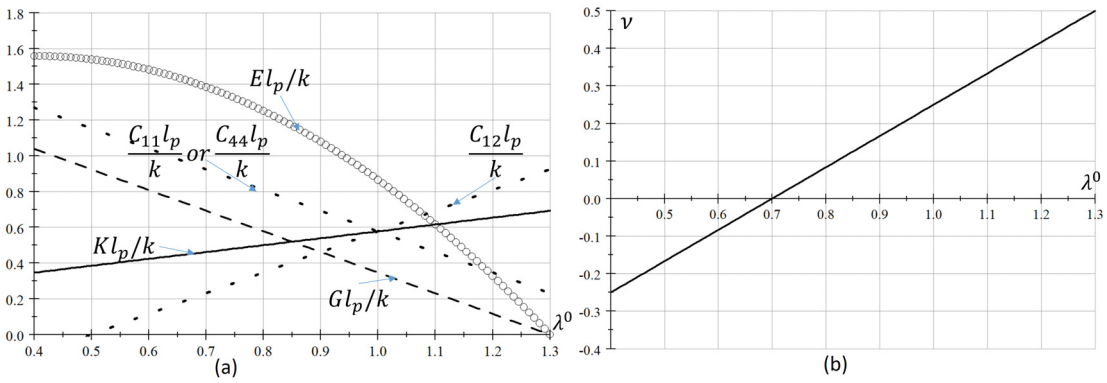

Fig. 5. The elastic constants versus the bond length ratio $\lambda^0 = r^0/(2l_p)$ for the body centered cubic (BCC) lattice: (a) the normalized elastic moduli and (b)the Poisson's ratio

effective elastic moduli in Fig. 5(a) are not constant for the lattice but change with λ^0 with the following features:

1. When $\lambda^0 = 1$, the normalized bulk modulus K, C_{11}, C_{12} and C_{44} share the same value of $1/\sqrt{3}$.
2. With the increase of λ^0 or the decrease of bond length, shear modulus μ, C_{11} and C_{44} linearly decrease, and μ reaches zero at $\lambda^0 = 1.3$ under the compression.
3. With the increase of λ^0 or the decrease of bond length, the Young's modulus quadratically decreases from the peak value at $\lambda^0 = 0.4$ to zero at $\lambda^0 = 1.3$.
4. With the increase of λ^0 or the decrease of bond length, C_{12} and K increases, and $C_{12} = 0$ at $\lambda^0 = 0.5$

Although the lattice is stable under the hydrostatic load with a positive K, when $\lambda^0 = 1.3$ where the bond is under a compression, the lattice loses stability for any shear strain with zero shear modulus, which is caused by the configurational force. This is different from buckling of the bond although we should consider buckling in actual applications as well. Therefore, when the ultimate compressive load to the lattice shall be determined by both buckling and configurational force.

Fig. 3(b) shows the Poisson's ratio. When $\lambda^0 = 1$, the Poisson's ratio $\nu = 0.25$, which is consistent with the literature (Laubie et al. 2017; Yin 2022). Generally, central-force lattices restrict the domain of application of the lattice element method (LEM) to isotropic materials exhibiting a Poisson's ratio of $\nu = 0.25$ in 3D (Laubie et al. 2017). To overcome this limitation, more advanced potentials other than a pair-wise potential were introduced. However, the singum model discloses that applying a prestress through the surface, the Poisson's ratio predicted by a pair-wise potential will shift from $\nu = 0.25$ to other values. When $\lambda^0 < 0.7$ the Poisson's ratio becomes negative. This discovery creates a feasibility to fabricate auxetic materials by using the prestresses. In addition, the stiffness of the lattice can be combined into the classic micromechanical models when both volumetric reinforcement and lattice reinforcement exist.

CONCLUSIONS

The singum model has been generalized to lattice metamaterials and composites for

prediction of the effective elasticity based on the stiffness of the lattice components with a linear elastic potential, in which the load is transferred through the lattice network represented by unit cells. The variational method is used to investigate the equilibrium of the singum and derive its averaged stress variation with strain. The following conclusions or discoveries have been observed:
(1) For both regular 2D honeycomb lattices and 3D BCC lattices, when a tensile prestress is applied, the Poisson's ratio can be negative.
(2) The shear modulus reduces with the compressive prestress and will cause the loss of stability by the configurational forces.
(3) For the auxetic lattices transformed by regular 2D honeycomb lattice, it can reach high negative Poisson's ratio, which is different in different loading orientation.
The singum model provides insight to fabricate new auxetic materials.

DATA AVAILABILITY STATEMENT

All data that support the findings of this study are available from the corresponding author upon reasonable request.

ACKNOWLEDGMENTS

This work is sponsored by the National Science Foundation IIP #1738802, IIP #1941244, CMMI #1762891, and U.S. Department of Agriculture NIFA #2021-67021-34201, whose support is gratefully acknowledged.

REFERENCES

Arruda, E. M. and Boyce, M. C. (1993). "A three-dimensional constitutive model for the large stretch behavior of rubber elastic materials." *Journal of the Mechanics and Physics of Solids*, 41(2), 389–412.

Boyce, M. C. and Arruda, E. M. (2000). "Constitutive models of rubber elasticity: a review." *Rubber chemistry and technology*, 73(3), 504–523.

Chen, Y., Scarpa, F., Liu, Y., and Leng, J. (2013). "Elasticity of anti-tetrachiral anisotropic lattices." *International Journal of Solids and Structures*, 50(6), 996–1004.

Gao, Y., Zhou, Z., Hu, H., and Xiong, J. (2021). "New concept of carbon fiber reinforced composite 3d auxetic lattice structures based on stretching-dominated cells." *Mechanics of Materials*, 152, 103661.

Gregg, C. E., Kim, J. H., and Cheung, K. C. (2018). "Ultra-light and scalable composite lattice materials." *Advanced Engineering Materials*, 20(9), 1800213.

Jang, S.-H. and Yin, H. (2015). "Effective electrical conductivity of carbon nanotube-polymer composites: a simplified model and its validation." *Materials Research Express*, 2(4), 045602.

Ju, J. and Chen, T. (1994). "Micromechanics and effective moduli of elastic composites containing randomly dispersed ellipsoidal inhomogeneities." *Acta Mechanica*, 103(1), 103–121.

Lakes, R. (1987). "Foam structures with a negative poisson's ratio." *Science*, 235, 1038–1041.

Laubie, H., Monfared, S., Radjaï, F., Pellenq, R., and Ulm, F.-J. (2017). "Effective potentials and elastic properties in the lattice-element method: isotropy and transverse isotropy." *Journal of Nanomechanics and Micromechanics*, 7(3), 04017007.

Li, K., Gao, X.-L., and Roy, A. (2003). "Micromechanics model for three-dimensional open-cell foams using a tetrakaidecahedral unit cell and castigliano's second theorem." *Composites Science and Technology*, 63(12), 1769–1781.

Mouritz, A. P., Bannister, M. K., Falzon, P., and Leong, K. (1999). "Review of applications for advanced three-dimensional fibre textile composites." *Composites Part A: applied science and manufacturing*, 30(12), 1445–1461.

Mura, T. (1987). *Micromechanics of defects in solids*. Springer Netherlands.

Saxena, K. K., Das, R., and Calius, E. P. (2016). "Three decades of auxetics research-materials with negative poisson's ratio: a review." *Advanced Engineering Materials*, 18(11), 1847–1870.

Šturcová, A., Davies, G. R., and Eichhorn, S. J. (2005). "Elastic modulus and stress-transfer properties of tunicate cellulose whiskers." *Biomacromolecules*, 6(2), 1055–1061.

Tucker III, C. L. and Liang, E. (1999). "Stiffness predictions for unidirectional short-fiber composites: review and evaluation." *Composites science and technology*, 59(5), 655–671.

Weinberger, C. R., Boyce, B. L., and Battaile, C. C. (2013). "Slip planes in bcc transition metals." *International Materials Reviews*, 58(5), 296–314.

Xiong, J., Mines, R., Ghosh, R., Vaziri, A., Ma, L., Ohrndorf, A., Christ, H.-J., and

Wu, L. (2015). "Advanced micro-lattice materials." *Advanced Engineering Materials*, 17(9), 1253–1264.

Yin, H. (2022). "A simplified continuum particle model bridging interatomic potentials and elasticity of solids." *ASCE Journal of Engineering Mechanics*, (in press).

Yin, H., Sun, L., and Chen, J. (2002). "Micromechanics-based hyperelastic constitutive modeling of magnetostrictive particle-filled elastomers." *Mechanics of materials*, 34(8), 505–516.

Yin, H. and Zhao, Y. (2016). *Introduction to the micromechanics of composite materials*. CRC press.